Structural basis for selective AMPylation of Rac-subfamily GTPases by *Bartonella* effector protein 1 (Bep1)

Nikolaus Dietz[a,1], Markus Huber[a,1], Isabel Sorg[a], Arnaud Goepfert[a,2], Alexander Harms[a], Tilman Schirmer[a,3], and Christoph Dehio[a,3]

[a]Biozentrum, University of Basel, 4056 Basel, Switzerland

Edited by Ralph R. Isberg, Tufts University School of Medicine, Boston, MA, and approved February 8, 2021 (received for review November 8, 2020)

Small GTPases of the Ras-homology (Rho) family are conserved molecular switches that control fundamental cellular activities in eukaryotic cells. As such, they are targeted by numerous bacterial toxins and effector proteins, which have been intensively investigated regarding their biochemical activities and discrete target spectra; however, the molecular mechanism of target selectivity has remained largely elusive. Here we report a bacterial effector protein that selectively targets members of the Rac subfamily in the Rho family of small GTPases but none in the closely related Cdc42 or RhoA subfamilies. This exquisite target selectivity of the FIC domain AMP-transferase Bep1 from *Bartonella rochalimae* is based on electrostatic interactions with a subfamily-specific pair of residues in the nucleotide-binding G4 motif and the Rho insert helix. Residue substitutions at the identified positions in Cdc42 enable modification by Bep1, while corresponding Cdc42-like substitutions in Rac1 greatly diminish modification. Our study establishes a structural understanding of target selectivity toward Rac-subfamily GTPases and provides a highly selective tool for their functional analysis.

AMPylation | structure function | FIC domain | RhoGTPases | Bartonella effector protein

Small GTPases of the Ras-protein superfamily are molecular switches that control fundamental cellular functions in eukaryotes by cycling between GTP-bound "on" and GDP-bound "off" conformational states of their switch regions 1 (Sw1) and 2 (Sw2) (1, 2). Members of the Ras-homology (Rho) protein family function as signaling hubs and regulate cytoskeletal rearrangements, cell motility, and the production of reactive oxygen species (3, 4). The defining element in Rho-family GTPases is the presence of a Rho insert, a highly variable, 13-residue-long, α-helical insert close to the C terminus. The Rho insert has previously been implicated in the wiring of Rho-family GTPases to their specific biological functions (5, 6). Six members of the Rho-protein family closely related to Cdc42 share an altered amino acid sequence in the G4 nucleotide binding motif with a glutamine residue instead of lysine in the second position.

Due to their central role in eukaryotic cell signaling, especially in the immune response, Rho-family GTPases are targeted by a plethora of bacterial virulence factors, including secreted bacterial toxins that autonomously enter host cells and effector proteins that are directly translocated from bacteria into host cells via dedicated secretion systems (7, 8). By means of these virulence factors, pathogens established ways to stimulate, attenuate, or destroy the intrinsic GTPase activity of Rho-family GTPases, either directly through covalent modification of residues in the Sw1 or Sw2 regions (8) or indirectly by mimicking guanine nucleotide exchange factor (GEF) or GTPase-activating protein (GAP) function. However, the structural basis for selective targeting of Rho-family GTPase subfamilies has remained unknown (7).

The bacterial genus *Bartonella* comprises a rapidly expanding number of virtually omnipresent pathogens adapted to mammals, many of which have been recognized to cause disease in humans (9). The stealth infection strategy of *Bartonella* spp. (10) rely to a large extent on translocation of multiple *Bartonella* effector proteins (Beps) via a dedicated type 4 secretion system. Strikingly, the majority of the currently known several dozens of Beps contains enzymatic FIC domains (9, 11), indicating that *Bartonella* spp. successfully utilize this effector type in their lifestyle. In order to gain more insights into the function of FIC domain-containing Beps we have here investigated Bep1 of *Bartonella rochalimae* originally described by Harms et al. (11).

Filamentation induced by cyclic AMP (FIC) domain-containing effector proteins belong to the ubiquitous FIC protein family with a conserved molecular mechanism for posttranslational modification of target proteins. FIC domains consist of six helices with a common HxFx(D/E)GNGRxxR motif between the central helices 4 and 5 (12). Some of the FIC domain-containing effector proteins have been recognized to modify Rho-family GTPases by catalyzing transfer of the AMP moiety from the ATP substrate to specific target hydroxyl side chains (12, 13). Prototypical examples are the effector proteins IbpA from *Histophilus somnii* and VopS from *Vibrio parahaemolyticus*, which both target a wide range of Rho-family GTPases and AMPylate (adenylylate) a conserved tyrosine or

Significance

Mammalian cells regulate diverse cellular processes in response to extracellular cues. Small GTPases of the Rho family act as molecular switches to rapidly regulate discrete cellular activities, such as cytoskeletal dynamics, cell movement, and innate immune responses. Numerous bacterial virulence factors modulate the function of Rho-family GTPases and thereby manipulate intracellular signaling. For many of these virulence factors we have gained detailed understanding how they covalently modify individual Rho-family GTPases to reprogram their activities; however, their mechanisms of selective targeting of distinct subsets of Rho-family GTPases remained elusive. Using a combination of structural biology and biochemistry, we demonstrate for the effector protein Bep1 exclusive specificity for Rac-subfamily GTPases and propose the underlying mechanism of target selectivity.

Author contributions: N.D., M.H., I.S., A.H., T.S., and C.D. designed research; N.D., M.H., I.S., A.G., and A.H. performed research; N.D., M.H., A.G., A.H., T.S., and C.D. analyzed data; and N.D., M.H., T.S., and C.D. wrote the paper.

The authors declare no competing interest.

This article is a PNAS Direct Submission.

[1]N.D. and M.H. contributed equally to this work.

[2]Present address: Ichnos Sciences Biotherapeutics SA, 1066 Epalinges, Switzerland.

[3]To whom correspondence may be addressed. Email: tilman.schirmer@unibas.ch or christoph.dehio@unibas.ch.

This article contains supporting information online at https://www.pnas.org/lookup/suppl/doi:10.1073/pnas.2023245118/-/DCSupplemental.

Published March 15, 2021.

threonine residue of Sw1, respectively (14–16). Both modifications result in abrogation of downstream signaling, causing collapse of the cytoskeleton of the host cell and subsequent cell death (17). Here we show that the FIC domain of *Bartonella* effector protein 1 of *B. rochalimae* (Bep1) AMPylates the same Sw1 tyrosine residue as IbpA, while the target spectrum is strictly limited to the Rac subfamily of Rho GTPases. Employing a combination of structural analysis, modeling, biochemistry, and mutational analysis, we identify the structural determinants of this remarkable target selectivity. Our findings highlight the potential of Bep1 as a tool for dissecting Rho-family GTPase activities and provide a rationale for the redesign of its target selectivity.

Results

Bep1 Selectively AMPylates Rac-Subfamily GTPases. Bep1 is composed of a canonical FIC domain followed by an oligosaccharide binding (OB) fold and a C-terminal BID domain (11). The latter domain is implicated in recognition and translocation by the type 4 secretion system VirB/VirD4 of *Bartonella* (18, 19).

In search for Bep1 targets we performed AMPylation assays by incubating lysates of *Escherichia coli* expressing Bep1 with eukaryotic cell lysates and α-P^{32}–labeled ATP and observed a radioactive band migrating with an apparent molecular weight of 20 kDa (*SI Appendix*, Fig. S1*A*), consistent with modification of Rho-family GTPases as previously described for IbpA and VopS (15, 16). To investigate further, we explored the target spectrum of Bep1 and compared it to those of the FIC domains of IbpA ($IbpA_{FIC2}$) or VopS ($VopS_{FIC}$) by selecting 19 members of the Ras superfamily (Fig. 1*A*) with an emphasis on members of the Rho family. While AMPylation activity of all three enzymes was strictly confined to Rho-family GTPases, their target selectivity spectra differed markedly: while Bep1 modified exclusively members of the Rac subfamily (i.e., Rac1/2/3 and RhoG), the target spectrum of $IbpA_{FIC2}$ comprised all Rho GTPases with the exception of RhoH/U/V and the Rnd subfamily, and $VopS_{FIC}$ was found to be fully indiscriminative (Fig. 1*A*, summarized in Fig. 1*D*).

Next, we designed a minimal $Bep1_{FIC}$ construct (residues 13 to 229) that proved sufficient for selective target modification. Bep1 belongs to the class I of FIC proteins that are regulated by a small regulatory protein, here BiaA, that inhibits FIC activity by inserting a glutamate residue (E33) into the ATP binding pocket (20). In order to improve expression level and stability, we coexpressed $Bep1_{FIC}$ with an inhibition relieved mutant (E33G) of BiaA, yielding the stabilized minimal AMPylation-competent $Bep1_{FIC}$/$BiaA_{E33G}$ complex, in short, $Bep1_{FIC}$*.

$Bep1_{FIC}$* efficiently AMPylates its targets, and the activity depends on the presence of the catalytic histidine (H170) of the signature motif (Fig. 1*B*), consistent with the canonical AMPylation mechanism (20). $Bep1_{Fic}$*, in contrast to $VopS_{Fic}$, does not AMPylate $Rac1_{Y32F}$ (Fig. 1*C*), indicating that $Bep1_{Fic}$* modifies Y32 of the Rac1 Sw1 as confirmed by mass spectrometry (*SI Appendix*, Fig. S1*C*). Thus, $Bep1_{Fic}$* catalyzes the equivalent modification as $IbpA_{Fic2}$ (15, 21), whereas VopS modifies T35 (16).

In contrast to the GDP form, GTP-loaded GTPases may not be amenable to FIC-mediated modification of Y32 since this residue is known to be involved in GTP binding via interaction with the γ-phosphate group (22) (*SI Appendix*, Fig. S2*D*). Indeed, exchanging GDP against GTP efficiently protected the GTP hydrolysis deficient mutant $Rac1_{Q61L}$ from modification, and the same effect was observed when replacing GDP bound to wild-type Rac1 with nonhydrolyzable GTPγS (*SI Appendix*, Fig. S2*C*). Thus, we conclude that GDP-loaded GTPases are the physiological targets of Bep1-mediated AMPylation.

The Crystal Structure of $Bep1_{FIC*}$ Reveals an Extended Target Recognition Flap. To reveal the structural basis of target selectivity, we solved the crystal structure of $Bep1_{FIC*}$ to 1.6 Å resolution. The structure (Fig. 2) closely resembles those of other FIC domains with AMPylation activity such as VbhT (20), IbpA (21), and VopS (23), featuring the active site defined by the conserved signature motif encompassing the α4–α5 loop and the N-terminal part of α5. Comparison with the apo crystal structure of the close Bep1 homolog from *Bartonella clarridgeiae* (Protein Data Bank [PDB] ID 4nps) shows that the presence of the small regulatory protein mutant BiaA (E33G) in $Bep1_{FIC*}$ does not affect the structure of the FIC domain (*SI Appendix*, Fig. S2*B*).

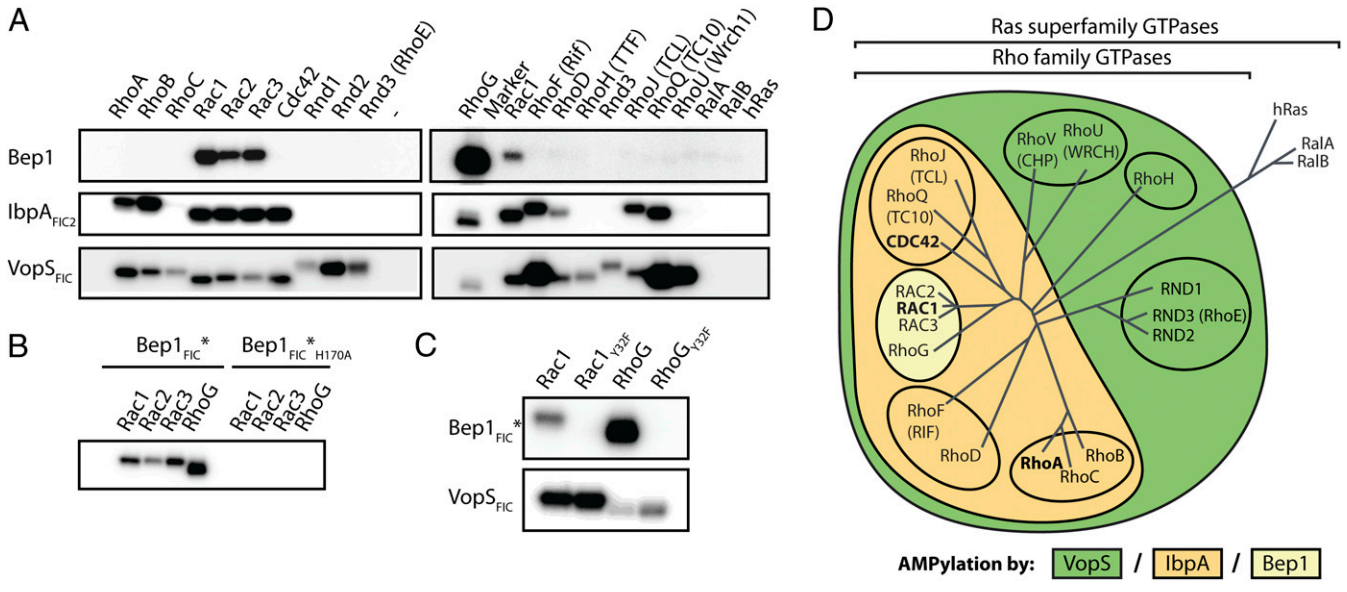

Fig. 1. Bep1 selectively targets Rac-subfamily GTPases. (*A*) ^{32}P-autoradiograms of in vitro AMPylation reactions using the indicated purified and GDP-loaded Rho-family GTPases display exquisite selectivity of full-length Bep1 for Rac-subfamily GTPases in contrast to the broader target spectrum of $IbpA_{FIC2}$ and $VopS_{FIC}$. (*B*) The FIC domain of Bep1 in complex with the regulatory protein BiaA ($Bep1_{FIC}$*) is sufficient for the recognition of Rac-subfamily GTPases and the catalytic H170 is required for AMPylation. (*C*) $Bep1_{FIC}$* AMPylates residue Y32 of Rac1 and RhoG since the respective Y32F mutants are not modified. AMPylation by the T35-specific $VopS_{FIC}$ indicates structural integrity of the analyzed GTPases and their Y32F mutants. (*D*) Venn diagram showing AMPylation target selectivity of tested FIC domains, overlaid to the phylogenetic relation of Rho-family GTPases (4).

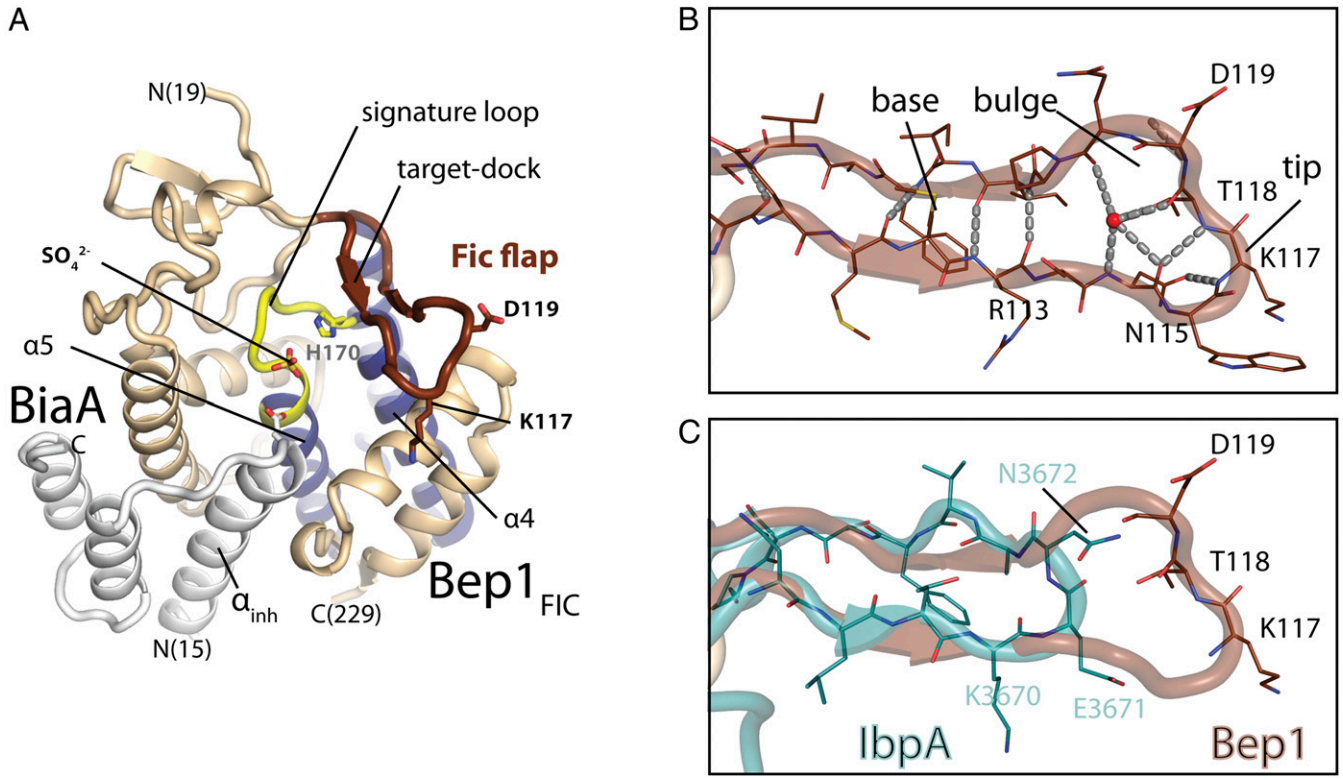

Fig. 2. Crystal structure of $Bep1_{FIC}$* reveals extended flap. (*A*) Cartoon representation of the crystal structure of the $Bep1_{FIC}$:BiaA complex ($Bep1_{FIC}$*) determined in this work. The regulatory protein BiaA is shown in light gray. The FIC domain fold is shown in light brown, with the central FIC helices (α4–α5) in blue. The FIC signature loop with the catalytic H170 is shown in yellow, and the FIC flap covering the active site is shown in dark brown. (*B*) Detailed view of the Bep1 flap region (PDB 5eu0; this study). Structural flap elements are stabilized by an H-bonding network involving main chain and side chain groups. H bonds are shown by gray dashed lines. The base of the flap forms a two-stranded β-sheet, with the N-terminal part constituting the target dock. The tip of the flap forms an i -> i + 3 turn between N115 and T118, which is further stabilized by the side chain of N115. The tip is followed by a bulge and a conserved proline residue and stabilized by interactions of the backbone with a central water (in red). This arrangement suggests that the well-defined structure of the flap orients side chains K117 and D119 for target interaction. (*C*) Overlay of flaps from $Bep1_{FIC}$ (brown) and $IbpA_{FIC2}$ (turquoise). Residues at the tips of both flaps are indicated. Compared to Bep1, the flap of IbpA is six residues shorter amounting to 8 Å (*SI Appendix*, Fig. S2*A*).

The active site is partly covered by a β-hairpin flap (Fig. 2*A*) that serves to register the segment carrying the modifiable side chain (here Sw1) to the active site via β-sheet augmentation, as has been inferred from bound peptides (16, 24), observed directly in the $IbpA_{FIC}$:Cdc42 complex (21), and discussed elsewhere (17). Strikingly, the flap of Bep1 and its orthologs in other *Bartonella* species (*SI Appendix*, Fig. S2*A*) is considerably longer than in other FIC structures (e.g., of $IbpA_{Fic2}$) and features a well-defined bulge at its tip (Fig. 2 *B* and *C*).

$Bep1_{FIC}$:Target Model Suggests That Charged Residues of the Flap Determine Target Selectivity. The complex structure of an FIC enzyme with a small GTPase target and the mechanism of FIC catalyzed AMPylation reaction has been elucidated for $IbpA_{FIC2}$ in complex with GDP-loaded Cdc42 (21) (Fig. 3*B*). The detailed view in Fig. 3*D* shows that the Sw1 segment of Cdc42 exhibits an extended conformation and forms antiparallel, largely sequence-independent, β-sheet interactions with the flap of the FIC enzyme, thereby aligning the modifiable Y32 with the active site. Considering the close structural homology of the catalytic core of $Bep1_{FIC}$ with $IbpA_{FIC2}$ (rmsd = 1.0 Å for 32 Cα atoms in the active site helices) and of Rac-subfamily GTPases with Cdc42 (rmsd = 0.44 Å for 175 Cα positions), we reasoned that computational assembly of a $Bep1_{FIC}$:Rac complex could provide a structural basis for an understanding of Bep1 target selectivity.

Fig. 3*A* shows the assembled $Bep1_{FIC}$:Rac2 complex that was obtained by individual superposition of 1) the $Bep1_{FIC}$ active site helices and the flap with the corresponding elements in $IbpA_{FIC2}$ and 2) the Sw1 loop of Rac2 with that of Cdc42. Thereby, we assumed implicitly that the interaction between these central segments should be very similar since both FIC enzymes utilize a homologous set of active residues to catalyze AMP transfer to a homologous residue (Y32) on Sw1.

The local structural alignment resulted in a virtually identical relative arrangement of the FIC core to the GTPase as in the template structure (compare Fig. 3 *A* and *B*) and caused no steric clashes. Conspicuously, the extended $Bep1_{FIC}$ flap is accommodated in a groove formed by Sw1 (residues 31 to 40), the GDP-loaded nucleotide binding G4 motif [T(K/Q)xD, residues 115 to 118] (25), and the following Rho-insert helix (Rac2 residues 121 to 133) (Fig. 3*C* and *SI Appendix*, Fig. S2*E*).

The manually created complex model was used as input for an adapted Rosetta modeling protocol to allow for sampling of backbone and side chain torsion angles in the interface of the complex, as described in *Materials and Methods* (26, 27). Consistent with the low affinity of the complex in vitro (see below), the models confirm the relatively small interface area of ~800 $Å^2$. Common to all top scoring models we find that the modifiable residue Y32 is pointing toward the active site of Bep1, where it is held in place by a main chain-mediated interaction between the base of the flap and the Sw1 loop of the GTPase (*SI Appendix*, Fig. S3*A*), indicating that the configuration of active site residues and the modifiable tyrosine side chain is, indeed, most likely the same as in the template complex.

However, in the $IbpA_{FIC2}$:Cdc42 complex, the aforementioned GTPase groove on the nucleotide binding face is not utilized for

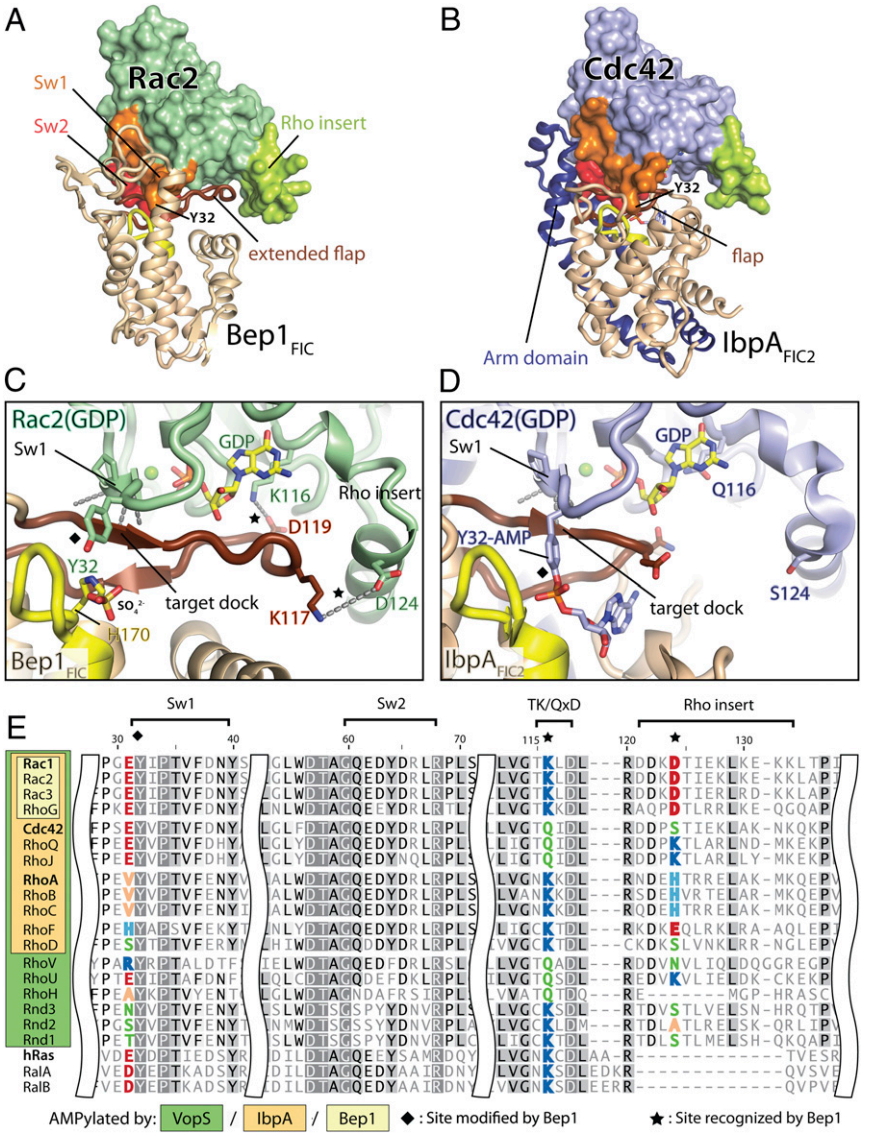

Fig. 3. $Bep1_{FIC}$:Rac2 complex model suggests charged interactions between FIC flap and targets. Side-by-side view of (*A*) $Bep1_{FIC}$:Rac2 complex model and (*B*) $IbpA_{FIC2}$:Cdc42 crystal structure (PDB 4itr). The FIC fold is shown in light brown. The FIC signature loop with the catalytic H170 is shown in yellow, and the FIC flap covering the active site is shown in brown. GTPases are shown as surface representation with indicated structural elements distinguished by color: Switch 1 (Sw1) in orange, Switch 2 (Sw2) in red, and Rho insert in green. The extension of the $Bep1_{FIC}$ flap is accommodated in a groove formed by the T(K/Q)xD motif and the Rho insert (*B*), whereas the arm domain of IbpA (in blue) contacts the effector binding regions, Sw1 and Sw2, of the GTPase. Comparison of intermolecular interactions in (*C*) the $Bep1_{FIC}$:Rac2 model and (*D*) the $IbpA_{FIC2}$:Cdc42 complex. H-bonding and electrostatic interactions are indicated by dashed lines in gray. The tip of the $Bep1_{FIC}$ flap is accommodated in a groove, with K117 and D119 in favorable position to interact with D124 and K116 of Rac2, respectively. (*D*) In the $IbpA_{FIC2}$:Cdc42 complex the Rho insert region is not involved in such interaction. (*E*) Structure-guided sequence alignment of the GTPases of the Rho, Ras, and RalA/B families. The K116/D124 configuration (marked with a star) is unique to Rac1/2/3 and RhoG (light yellow). Residue numbers refer to Rac1, and names of representative members of Rho subfamilies are indicated in bold.

the contact (Fig. 3*D*). Instead, the so-called arm domain of $IbpA_{FIC2}$ (Fig. 3*B*) constitutes a major part of the interface and contacts the highly conserved Sw2 loop of Cdc42. This rationalizes the broad target spectrum of arm domain-containing FIC AMP transferases like IbpA and VopS (12, 23). In turn, residues of the groove predicted to get recognized exclusively by $Bep1_{FIC}$ are likely to be important for the limited target range of Bep1. Conspicuously, the top scoring models revealed two potential salt bridges between the Bep1 flap and the Rac2 groove, namely, D119(Bep1)–K116(Rac2) and K117(Bep1)–D124(Rac2) (Fig. 3*C* and *SI Appendix*, Fig. S3*A*). Since the combination of K116 and D124 is exclusively found in the Rac subfamily as revealed by sequence alignment of Rho-family GTPases (Fig. 3*E*), we reasoned that these residues may contribute significantly to the specific recognition of Rac GTPases by Bep1 (Fig. 1*A*).

Two Salt Bridges between Flap and Target Are Crucial for Selective Interaction of $Bep1_{FIC}$ with Rac-Subfamily GTPases. The relevance of the two identified salt bridges in the $Bep1_{FIC}$*:Rac2 complex (Fig. 3*C*) for affinity and selectivity was tested by single and double replacements of the constituting residues 116 and 124 in a Bep1 target and a nontarget GTPase. For Rac1, we tested if substitutions at these residues with corresponding amino acids of Cdc42—a nontarget of Bep1 with the highest conservation in regions flanking the proposed interaction sites (Fig. 3*E*)—influence target recognition (loss-of-function approach; see interaction

schemes in Fig. 4*A*). In addition, we tested whether Cdc42 can be converted to a Bep1 target by reciprocal substitution(s) of these sites with the corresponding Rac1 residues (gain-of-function approach; Fig. 4*B*).

First, we applied, as for Fig. 1*A*, the autoradiography end-point assay with ^{32}P-α-ATP as substrate. Compared to wild-type Rac1, mutant D124S showed no significant difference in the amount of AMPylated target, whereas AMPylation of mutant K116Q and, even more, of the double mutant was found drastically reduced (Fig. 4*C* and *SI Appendix*, Fig. S4*A*). Conversely, in the gain-of-function approach, Cdc42 mutant S124D did not convert the GTPase to a Bep1 target, while mutant Q116K and the double mutant showed low but significant AMPylation (Fig. 4*D* and *SI Appendix*, Fig. S4*B*). In a fairly undiscriminating way, IbpA$_{FIC2}$ modified all investigated GTPase variants (*SI Appendix*, Fig. S4 *C* and *D*) indicating their proper folding. Together, the semiquantitative radioactive end-point assay demonstrated a major role of K116 in target recognition by Bep1$_{FIC}$*, while a contribution of D124 could not be demonstrated.

To overcome the limitations of the radioactive end-point assay and to characterize target AMPylation quantitatively, we developed an online ion exchange chromatography (oIEC) assay (*Materials and Methods*) which allows separation of reaction components (Fig. 4*E*) and efficient acquisition of enzymatic progress curves to determine initial velocities, v_{init} (see, for instance, *SI Appendix*, Fig. S4*F*, Inset). For AMPylation of Rac1 by Bep1$_{Fic}$*, titration experiments yielded K_M values of 0.52 and 1.4 mM for the substrates ATP and Rac1, respectively, and a k_{cat} of 1.9 s^{-1}. The comparison with published values on other Fic AMP transferases (*SI Appendix*, Table S1) shows that the K_M values are comparable to IbpA but that k_{cat} is smaller by about two orders of magnitude.

Considering the physiological conditions in the cell with an ATP concentration above K_M, Bep1 can be expected to be saturated with ATP and only partially loaded with the target (target concentration << $K_{M,\ target}$). In such a regime, the AMPylation rate will be given by

$$v = \frac{k_{cat}}{K_{M,target}} \times [E_0] \times [target]$$

(28), i.e., will depend solely on the second order rate constant $k_{cat}/K_{M,target}$ (efficiency constant), which is, thus, the relevant parameter for enzyme comparison.

Next, we determined the efficiency constants for all GTPase variants. In the loss-of-function series, the single mutants reduced the efficiency constant by 2- and 6-fold, and the double mutant reduced the efficiency constant by about 30-fold (Fig. 4*E* and *SI Appendix*, Table S1).

Under the assumptions that 1) k_{cat} is not changed upon the mutations, since they affect sites on the target that are distant from the catalytic center, and 2) K_M is equal to the K_D of the enzyme–target complex, as is warranted for a slow enzyme, the difference in the measured efficiency constants can be attributed to an altered stability of the Michaelis–Menten complex.

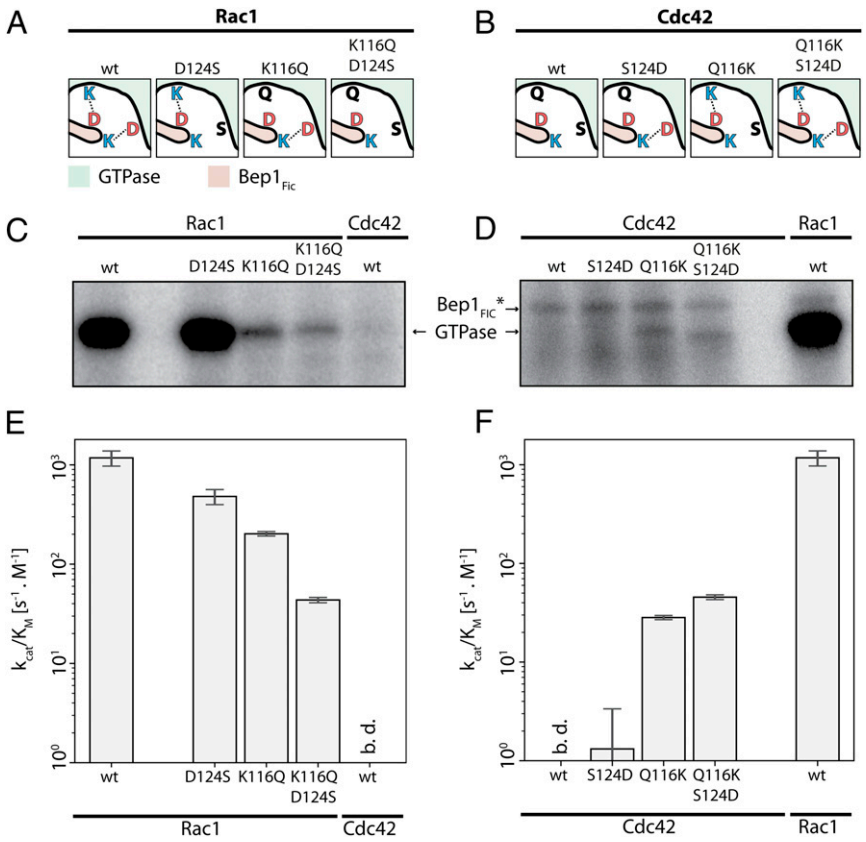

Fig. 4. Two salt bridges are crucial for Rac-subfamily selective AMPylation. (*A*) Schematic view of the two intramolecular Bep1$_{FIC}$:Rac1 salt bridges (*Left*) and their partial disruption upon site-directed Rac1 mutagenesis, yielding Rac1 loss-of-function mutants (*Right*). (*B*) Absence of ionic interactions in the predicted Bep1$_{FIC}$:Cdc42 interface (*Left*) and partial establishment of salt bridges in Cdc42 gain-of-function mutants (*Right*). (*C* and *D*) AMPylation of the variants given in *A* and *B* as measured by autoradiography. Note that due to the employed higher Bep1$_{FIC}$* concentration (*Material and Methods*), the experiments in *D* also revealed auto-AMPylation of Bep1$_{FIC}$*. (*E* and *F*) Enzymatic efficiency constants, k_{cat}/K_M, for Bep1$_{FIC}$* catalyzed AMPylation of the GTPase variants shown in *A* and *B* as derived from the oIEC measurements shown in *SI Appendix*, Fig. S4. b.d., below detection limit. Error bars indicate standard deviation of reaction efficiencies.

Furthermore, the change of the free energy of binding upon mutation ($\Delta\Delta G$) can be derived from the measured efficiency constants of wild-type and mutant target under these assumptions. The calculations given in *SI Appendix*, Table S2, show that the ΔΔG of the double mutant is larger by only about 25% compared to the $\Delta\Delta G$ sum of the single mutants, suggesting that the contributions of the two salt bridges are largely independent.

In the gain-of-function series, wild-type Cdc42 showed no and mutant S124D only marginal modification, while mutant Q116K showed a significant (about 30-fold larger than that of S124D) effect. Again, as in the previous series, the double mutant showed the largest effect (Fig. 4*F* and *SI Appendix*, Table S1).

Summarizing, the quantitative oIEC assay confirmed the prominent dependence of $Bep1_{FIC}$* catalyzed target modification on the type of residue in target position 116 that had already been revealed by the radioactive endpoint assay and predicted by modeling (*SI Appendix*, Fig. S3*A*) but also demonstrated a significant influence of the residue in position 124, such that both salt bridges appear to be crucial for efficient Bep1-mediated AMPylation of Rac-subfamily GTPases.

Discussion

Single residue alterations in the effector loop (switch I region) of Ras-family GTPases can alter the specificity for interaction with downstream effectors in cellular signaling cascades (29). Several protein interaction modes have been described for Rho-family GTPases (30, 31), even though the basis of discrimination between these structurally conserved but functionally diverse GTPases remained elusive. The highly divergent Rho insert has been linked to a number of biological effects, such as membrane ruffling, Rho kinase activation by RhoA (32, 33), or the interaction of Rac with the NADPH oxidase complex (34). However, these studies relied on deletion of the Rho insert, and it is unclear if respective mutant proteins were properly folded. More recent structural work on complexes between Formins (mDia and FMNL2) and RhoC (35) or Cdc42 (36, 37) show the direct involvement of the C-terminal residues of the Rho insert in complex formation. While the Rho insert contributes only marginally to RhoC:mDia complex formation (35), it is crucial for interaction specificity in the FMNL2:Cdc42 complex (36). Our structure–function analysis substantially augments this body of work and demonstrates that target selectivity of Bep1 for Rac-subfamily GTPases is encoded by intermolecular interaction with a different set of Rho-family specific structural elements: Bep1 interacts with N-terminal residues of the Rho-insert helix as well as the G4 motif residues. The observation that Cdc42 cannot be converted fully to a Rac1-like Bep1 target by the respective residue substitutions suggests additional, yet unknown, structural or dynamic features that contribute to efficient AMPylation.

Remarkably, Bep1's selectivity is based by and large on a short insert of six residues in the conserved lid loop of the FIC domain (Fig. 2*C*). This simple, yet elegant, evolutionary treat equips *Bartonella* with a precise molecular tool to interfere specifically with host signaling. As such, Bep1 is the first bacterial effector to selectively target Rac-subfamily GTPases without affecting the Rho or Cdc42 GTPase subfamilies. Insertions of few amino acids in loop regions as exemplified by Bep1 are found in other Fic proteins; however, their functional consequences are hard to predict based on sequences alone. However, it is conceivable that they contribute to the specificity for different target spectra. Targeting a broad range of Rho GTPases seems to require a more complex addition to the FIC domain as exemplified by the arm domain found in IbpA or VopS (Fig .3 *A* and *B*).

We speculate that in the infection process of *Bartonella*, the selective inactivation of Rac-subfamily GTPases plays a critical role for the evasion of the innate immune response, without causing the collateral damage and activation of the immune system associated with effectors that target a broad-spectrum of Rho GTPases, such as VopS or IbpA. In fact, Rac-subfamily selective AMPylation does not trigger a response of the innate immune system via activation of the pyrin inflammasome, which has been shown to accompany RhoA inactivation by covalent modification in the Sw1 region (38). Thus, avoiding RhoA inactivation may provide a substantial benefit for *Bartonella* to establish a largely asymptomatic chronic infection in their host.

Patients with impaired signaling of Rac-subfamily GTPases cannot clear bacterial infections due to diminished ability for ROS production in immune cells, as seen in patients suffering from chronic granulomatosis disease or case studies from patients with dysfunctional Rac2 genes resulting in neutrophil immunodeficiency syndrome (39, 40). Along these lines, we speculate that selective targeting of GDP-complexed Rac-subfamily GTPases provides the additional benefit that protein levels of GDP-bound Rac are not down-regulated via proteasomal degradation (41), resulting in a stable pool of inactive Rac subfamily GTPases that would subdue Rac-mediated immune responses effectively.

Beyond providing a molecular understanding for target selectivity among Rho-family GTPases, the narrow target spectrum of Bep1 for Rac-subfamily GTPases also provides a unique tool for dissecting their specific functions in cellular processes, such as cytoskeletal rearrangements related to the Rac1-dependent formation of membrane ruffles, the Rac2/RhoG-dependent production of reactive oxygen in immune cells, or the role of Rac1 in carcinogenesis.

Considering the simple topology and small size of the FIC domain, we find a surprisingly modular division of functions. While the conserved catalytic core allows efficient AMPylation of a target hydroxyl residue located in an extended loop that registers to the active site via β-strand augmentation, target affinity and thereby selectivity is encoded separately in a short loop insertion. The modular nature and amenable size of this structural framework appears well suited for the rational design of synthetic Rho-subfamily selective FIC domain AMP transferases with novel physiological activities and beyond.

Materials and Methods

Protein Expression and Purification. The FIC domain of Bep1 was cloned, expressed and purified in complex with the inhibition-relieved regulatory protein $BiaA_{E33G}$ as described for the crystallization construct and is subsequently referred to as $Bep1_{FIC}$*. For the generation of cleared bacterial lysate, the bacterial pellet was resuspended in reaction buffer (50 mM Tris·HCl, pH 8.0, 150 mM NaCl, 5 mM $MgCl_2$) supplemented with protease inhibitor mixture (complete EDTA-free mini, Roche) and lysed by sonication. After clearing the lysates by centrifugation (120,000 × *g* for 30 min at 4 °C), the supernatant was directly used in the assays or stored at −20 °C. Protein expression and purification of GST- or HIS-tagged GTPases and GST-tagged FIC domains of VopS and IbpA followed standard GST- or HIS-fusion-tag protocols. In short, *E. coli* BL21 or BL21 AI (Invitrogen) were transformed with expression plasmids and used for protein expression. Bacteria were grown in LB medium supplemented with appropriate antibiotic on a shaker until A_{600} = 0.6 to 0.8 at 30 °C. Protein expression was induced by addition of 0.2 mM isopropyl-β-D-thiogalactopyranoside (IPTG) (AppliChem GmbH) or 0.1% wt/vol arabinose (Sigma-Aldrich) for 4 to 5 h at 22 °C.

Bacteria were harvested by centrifugation at 6,000 × *g* for 6 min at 4 °C, resuspended in lysis buffer (20 mM Tris·HCl, pH 7.5, 10 mM NaCl, 5 mM $MgCl_2$, 1% Triton X-100, 5 mM DTT and protease inhibitor mixture [protean Mini EDTA-free, Roche]), and lysed using a French press (Thermo Fisher). After ultracentrifugation at 120,000 × *g* for 20 min at 4 °C the cleared lysate of GST-tagged GTPases was added to equilibrated glutathione-Sepharose resin (Genescript) and incubated for 1 h at 4 °C on a turning wheel. After four washing steps with wash buffer (20 mM Tris·HCl, pH 7.5, 10 mM NaCl, 5 mM $MgCl_2$) the bound protein was eluted with wash buffer supplemented with 10 mM reduced glutathione (Sigma-Aldrich).

Cleared lysate of HIS-tagged GTPases was injected on HisTrap HP columns (GE Healthcare) after equilibration with binding buffer (50 mM Hepes, pH 7.5, 150 mM NaCl, 5 mM $MgCl_2$, 20 mM imidazole). Washing with 10 column volumes of binding buffer was followed by elution with 5 column volumes of elution buffer (50 mM Hepes, pH 7.5, 150 mM NaCl, 5 mM $MgCl_2$, 500 mM imidazole). HIS-tagged GTPases were incubated with 50 mM EDTA and further

purified by size exclusion chromatography (HiLoad 16/600 Superdex 75 pg, GE Healthcare) with SEC buffer (50 mM Hepes, pH 7.5, 150 mM NaCl, 5 mM $MgCl_2$, 50 mM EDTA). EDTA was removed by buffer exchange (50 mM Hepes, pH 7.5, 150 mM NaCl, 5 mM $MgCl_2$) and the protein used for quantitative AMPylation assays.

Nucleotide Loading of GTPases. To preload purified GTPases with the respective nucleotide, 50 μM protein was incubated with 3 mM nucleotide (GDP, GTP, GTPγS, or GMP-PNP) and 8 mM EDTA in reaction buffer (50 mM Tris·HCl, pH 8.0, 150 mM NaCl, 5 mM $MgCl_2$) for 20 min at room temperature. Then 16 mM $MgCl_2$ was added to stop the nucleotide exchange. The protein was then used for both in vitro AMPylation assays.

Radioactive AMPylation Assay. The in vitro AMPylation activity was assayed using either cleared bacterial lysates expressing full-length Bep1 or purified FIC domains of Bep1, VopS, and IbpA.

To analyze the AMPylation activity of Bep1, $Bep1_{FIC}$*, $VopS_{FIC}$, and $IbpA_{FIC2}$, 10 μM purified GTPase, preloaded with respective nucleotide, was incubated in presence of the respective AMPylator with 10 μCi [α-^{32}P]-ATP (Hartmann Analytic) in reaction buffer (50 mM Tris·HCl, pH 8.0, 150 mM NaCl, 5 mM $MgCl_2$ containing 0.2 mg/mL RNaseA) for 1 h at 30 °C. The reaction was stopped by addition of SDS-sample buffer and heating to 95 °C for 5 min. Samples were separated by SDS-PAGE and subjected to autoradiography.

For AMPylation of Rac1, Cdc42, and their mutant variants, 5 μM of purified HIS-tagged GTPases, preloaded with GDP, were incubated with $Bep1_{FIC}$* (1 and 5 μM in Rac1 and Cdc42 variants, respectively) in the presence of [α-^{32}P]-ATP (Hartmann Analytic) for 40 min in reaction buffer (50 mM Tris·HCl, pH 8.0, 150 mM NaCl, 5 mM $MgCl_2$) at 20 °C.

Quantitative AMPylation Assay. We employed an oIEC assay, monitoring the UV absorption of GTPase targets at 260 nm. The observed increase in absorbance due to AMPylation could be readily quantified and resulted in progress curves that yielded reaction velocities and in turn AMPylation efficiencies (k_{cat}/K_M).

A 1-mL Resource Q column (GE Healthcare) was equilibrated with loading buffer (20 mM Tris/HCl, pH 8.5 or 6.5 for Rac1 or Cdc42, respectively). The purified GTPase variant was mixed with $Bep1_{FIC}$* in reaction buffer (50 mM Tris·HCl, pH 7.5, 150 mM NaCl, 5 mM $MgCl_2$) in a large volume (200 μL), and the reaction was started at t = 0 by addition of 3.2 mM ATP (final concentration, supplemented with 6.4 mM $MgCl_2$). A small fraction (20 μL) of the reaction mixture was injected automatically on the column at intervals of 6 min. After washing with loading buffer, a gradient of elution buffer [1 M $(NH_4)_2SO_4$ in loading buffer] was applied, yielding a chromatogram for each injection.

Reaction progress was monitored by quantification of GTPase peak area measured at 260 nm from each chromatogram by numerical peak integration. Note that this peak comprised both native and AMPylated GTPase. A heuristic quadratic function was fitted to the progress curves to yield the initial velocity. Calibration with ATP samples of known concentrations allowed to derive absolute AMPylation velocities. Enzymatic K_M and k_{cat} parameters were derived from v_{init}(S) type Michaelis–Menten plots (*SI Appendix*, Fig. S4 *F* and *G*). Depending on the activity, $Bep1_{FIC}$* concentrations were chosen such that the enzyme velocities were kept within a similar range (*SI Appendix*, Fig. S4 *H* and *I*). Nominal GTPase concentrations were corrected based on the back-extrapolated peak absorbance at t = 0. Fitting of single-substrate kinetic measurements by the Michaelis–Menten equation was developed in python 3 with standard modules provided in the Anaconda distribution.

Crystallization and Structure Determination. The full-length *biaA* gene that codes for the small ORF directly upstream of *bep1* gene and part of the *bep1* gene from *B. rochalimae* encoding the FIC domain (amino acid residues 13 to 229) were PCR amplified from genomic DNA. The PCR products for *biaA* and the fragment of *bep1* were cloned into the vector pRSF-Duet1. pRSF-Duet1 containing *biaA* or *bep1* were introduced into *E. coli* BL21 (DE3) by transformation. The constructs were expressed and purified as described for VbhA/VbhT(FIC) (20) with the difference that 5 mM DTT was additionally used throughout the purification procedure. Fractions were pooled and concentrated to 13.6 mg mL^{-1} for crystallization.

Crystals were obtained at 4 °C using the hanging-drop vapor diffusion method upon mixing 1 μL protein solution with 1 μL reservoir solution. The reservoir solution was composed of 0.2 M Hepes (pH 7.5), 2.3 M ammonium sulfate, and 2% vol/vol PEG 400. For data collection, crystal was frozen in liquid nitrogen without additional cryoprotectant. Diffraction data were collected on beam-line X06SA (PXIII) of the Swiss Light Source (λ = 1.0 Å) at 100 K on a MAR CCD detector. Data were processed with XDS and the structure solved by molecular replacement with Phaser (42) using the VbhA/VbhT(FIC) structure (PDB 3SHG) as search model. Several rounds of iterative model building and refinement were performed using Coot (43) and Buster (44), respectively. The final structure shows high similarity to the VbhA/VbhT(FIC) structure (rmsd 1.44 Å for 183 Cα positions). Crystallographic data are given in *SI Appendix*, Table S3. Figs. 2 *A–C* and 3 *A–D* and *SI Appendix*, Figs. S2 *B* and *D–F* and S3*A* have been generated using Pymol (45).

Homology Modeling of the Bep1:Target Complex and Generation of Structure-Based Sequence Alignments. The input structure for homology modeling was chosen from all available Rac-subfamily structures (i.e., Rac1-3 and RhoG). In total, 43 PDB entries were analyzed (*SI Appendix*, Table S4). Cdc42 (chain D) of the IbpA–Cdc42 complex served as reference for all superimpositions. The superimposition was carried out in two steps: a global superimposition over all Cα atom positions and a second, local superimposition using all atom positions of residues 27 to 37 (Sw1) of Cdc42. Both steps used the align–algorithm implemented in Pymol (version 1.8) with standard settings.

We observed high structural agreement between Rac-subfamily GTPase structures in the PDB and the reference chain with an average Cα rmsd below 0.5 Å. In contrast, we noticed large variations in the all-atom rmsds of residues in the Sw1 region that correlate with the nucleotide state of the GTPase. In order to find the most suitable PDB for homology modeling we searched for the smallest coordinate deviations to the Sw1 conformation of the Cdc42 reference chain: three GDP-loaded GTPase structures display an rmsd of coordinates to the template below 1 Å (*SI Appendix*, Table S4). Two of these structures are complexes of the Rho-GDP-dissociation inhibitor (RhoGDI) with either Rac1 (PDB ID 1hh4) or Rac2 (PDB ID 1ds6) representing the cytosolic storage form of the GTPases. The third structure is the Zn^{2+}-bound trimeric form of Rac1 (PDB: 2P2L), in which Sw1 is involved in the Zn^{2+}-mediated trimer interface. From these candidate PDBs, we chose 1ds6 as the most appropriate for homology modeling since it represents a physiological state of a Rac-GTPase (in contrast to 2P2L). Further, 1ds6 features a fully resolved Sw1 region and a higher resolution compared to entry 1hh4. To correspond closely to the reference structure, we built an alternative standard rotamer for the solvent-exposed Y32 of Rac2 in the PDB 1ds6 (Fig. 3*C*). The FIC domains of Bep1 and IbpA were superimposed using the C-α atom positions of flap residues that adopt β-sheet–like conformations in order to mimic the catalytically active conformation of the IbpA:Cdc42 complex. Superimposing $IbpA_{FIC2}$ residues 3,667 to 3,670 and 3,673 to 3,677, corresponding to Bep1 residues 110 to 113 and 122 to 126, respectively, yields an rms error of 0.87 Å for 9 CA pairs.

Modeling of the complex structure was carried out using the manually selected, superimposed, and curated model described above as starting structure for an adapted flexDDG protocol (26) implemented in the Rosetta package. In short, ligands (GDP and hydrated Mg^{2+}) and ordered water molecules (as found in PDB entry 1ds6, as well as one water molecule in the center of the Bep1 flap, shown in Fig. 2*B*) that are part of the protein complex interface were parameterized for the use in Rosetta and included in the modeling process to increase precision and validity of the resulting models. The selected small molecules had been refined with B factors that are comparable to neighboring main chain atoms in the respective PDB entries (1ds6 and 5eu0). Next, the curated input model is subjected to a global minimization of backbone and side chain torsions in Rosetta (Minimize step) followed by local sampling of backbone and side chain degrees of freedom for all residues with C-β atoms within 10 Å distance of Rac2 residue D124 (Backrub step). The side chains of the resulting models are optimized globally (Packing step), and backbone and side chain torsion energies are minimized globally (Minimize step 2). Finally, models are scored on the all-atom level using the suggested talaris_2014 function (26), and best scoring models were analyzed visually. The recommended total of 35 independent simulations is calculated for the complex with a maximum number of 5,000 minimization iterations (convergence limit score 1.0) and 35,000 backrub trial steps each.

Structure guided multiple sequence alignments (MSA) were generated by manual adjustment of MSA generated using the ClustalW algorithm as implemented in the GENEIOUS software package (46) version 7.1.7.

Quantification and Statistical Analysis. Statistical parameters are given in *SI Appendix*, Tables S1 and S2 . Error bars in quantitative AMPylation assays show the SD of reaction efficiencies (k_{cat}/K_M) derived from the least-square minimization of the fitting routine.

Data and Software Availability. Data analysis of oIEC was performed with python3 scripts made available under https://github.com/FicTeam/HuberDietz_PNAS21. Protein structure data have been deposited in Protein Data Bank under accesion number 5EU0.

ACKNOWLEDGMENTS. We thank the laboratories of Klaus Aktories, Kim Orth, and Seema Mattoo for providing expression constructs of Rho-family GTPases, VopS, and IbpA, respectively. We thank the beamline staff at the Swiss Light Source in Villigen for expert help in data acquisition. Rosetta modelling calculations were performed at sciCORE (https://scicore.unibas.ch/) scientific computing core facility at University of Basel. This work was supported by grant 310030A_173119 from the Swiss National Science Foundation (http://www.snf.ch/en/Pages/default.aspx) and advanced grant 340330 (FicModFun) from the European Research Council, both to C.D.

1. J. Didsbury, R. F. Weber, G. M. Bokoch, T. Evans, R. Snyderman, rac, a novel ras-related family of proteins that are botulinum toxin substrates. *J. Biol. Chem.* **264**, 16378–16382 (1989).
2. K. Wennerberg, K. L. Rossman, C. J. Der, The Ras superfamily at a glance. *J. Cell Sci.* **118**, 843–846 (2005).
3. A. B. Jaffe, A. Hall, Rho GTPases: Biochemistry and biology. *Annu. Rev. Cell Dev. Biol.* **21**, 247–269 (2005).
4. S. J. Heasman, A. J. Ridley, Mammalian Rho GTPases: New insights into their functions from in vivo studies. *Nat. Rev. Mol. Cell Biol.* **9**, 690–701 (2008).
5. G. M. Bokoch, B. A. Diebold, Current molecular models for NADPH oxidase regulation by Rac GTPase. *Blood* **100**, 2692–2696 (2002).
6. A. E. Karnoub, M. Symons, S. L. Campbell, C. J. Der, Molecular basis for Rho GTPase signaling specificity. *Breast Cancer Res. Treat.* **84**, 61–71 (2004).
7. K. Aktories, Bacterial protein toxins that modify host regulatory GTPases. *Nat. Rev. Microbiol.* **9**, 487–498 (2011).
8. K. Aktories, Rho-modifying bacterial protein toxins. *Pathog. Dis.* **73**, ftv091 (2015).
9. A. Wagner, C. Dehio, Role of distinct type-IV-secretion systems and secreted effector sets in host adaptation by pathogenic Bartonella species. *Cell. Microbiol.* **21**, e13004 (2019).
10. A. Harms, C. Dehio, Intruders below the radar: Molecular pathogenesis of *Bartonella* spp. *Clin. Microbiol. Rev.* **25**, 42–78 (2012).
11. A. Harms *et al*., Evolutionary dynamics of pathoadaptation revealed by three independent acquisitions of the VirB/D4 type IV secretion system in Bartonella. *Genome Biol. Evol.* **9**, 761–776 (2017).
12. A. Harms, F. V. Stanger, C. Dehio, Biological diversity and molecular plasticity of FIC domain proteins. *Annu. Rev. Microbiol.* **70**, 341–360 (2016).
13. C. Hedberg, A. Itzen, Molecular perspectives on protein adenylylation. *ACS Chem. Biol.* **10**, 12–21 (2015).
14. S. Mattoo *et al*., Comparative analysis of *Histophilus somni* immunoglobulin-binding protein A (IbpA) with other fic domain-containing enzymes reveals differences in substrate and nucleotide specificities. *J. Biol. Chem.* **286**, 32834–32842 (2011).
15. C. A. Worby *et al*., The fic domain: Regulation of cell signaling by adenylylation. *Mol. Cell* **34**, 93–103 (2009).
16. M. L. Yarbrough *et al*., AMPylation of Rho GTPases by *Vibrio* VopS disrupts effector binding and downstream signaling. *Science* **323**, 269–272 (2009).
17. C. R. Roy, J. Cherfils, Structure and function of Fic proteins. *Nat. Rev. Microbiol.* **13**, 631–640 (2015).
18. R. Schulein *et al*., A bipartite signal mediates the transfer of type IV secretion substrates of Bartonella henselae into human cells. *Proc. Natl. Acad. Sci. U.S.A.* **102**, 856–861 (2005).
19. A. Wagner, C. Tittes, C. Dehio, Versatility of the BID domain: Conserved function as type-IV-secretion-signal and secondarily evolved effector functions within *Bartonella*-infected host cells. *Front. Microbiol.* **10**, 921 (2019).
20. P. Engel *et al*., Adenylylation control by intra- or intermolecular active-site obstruction in Fic proteins. *Nature* **482**, 107–110 (2012).
21. J. Xiao, C. A. Worby, S. Mattoo, B. Sankaran, J. E. Dixon, Structural basis of Fic-mediated adenylylation. *Nat. Struct. Mol. Biol.* **17**, 1004–1010 (2010).
22. K. Lapouge *et al*., Structure of the TPR domain of p67phox in complex with Rac.GTP. *Mol. Cell* **6**, 899–907 (2000).
23. P. Luong *et al*., Kinetic and structural insights into the mechanism of AMPylation by VopS Fic domain. *J. Biol. Chem.* **285**, 20155–20163 (2010).
24. A. Goepfert, F. V. Stanger, C. Dehio, T. Schirmer, Conserved inhibitory mechanism and competent ATP binding mode for adenylyltransferases with Fic fold. *PLoS One* **8**, e64901 (2013).
25. A. Wittinghofer, I. R. Vetter, Structure-function relationships of the G domain, a canonical switch motif. *Annu. Rev. Biochem.* **80**, 943–971 (2011).
26. K. A. Barlow *et al*., Flex ddG: Rosetta Ensemble-based estimation of changes in protein-protein binding affinity upon mutation. *J. Phys. Chem. B* **122**, 5389–5399 (2018).
27. G. T. Gapp *et al*., Control of protein signaling using a computationally designed GTPase/GEF orthogonal pair. *Proc. Natl. Acad. Sci. U.S.A.* **109**, 5277–5282 (2012).
28. A. G. Marangoni, *Enzyme Kinetics: A Modern Approach* (Wiley, Hoboken, NJ, 2002).
29. C. Herrmann, Ras-effector interactions: After one decade. *Curr. Opin. Struct. Biol.* **13**, 122–129 (2003).
30. I. R. Vetter, A. Wittinghofer, The guanine nucleotide-binding switch in three dimensions. *Science* **294**, 1299–1304 (2001).
31. R. Dvorsky, M. R. Ahmadian, Always look on the bright site of Rho: Structural implications for a conserved intermolecular interface. *EMBO Rep.* **5**, 1130–1136 (2004).
32. A. E. Karnoub, C. J. Der, S. L. Campbell, The insert region of Rac1 is essential for membrane ruffling but not cellular transformation. *Mol. Cell. Biol.* **21**, 2847–2857 (2001).
33. H. Zong, K. Kaibuchi, L. A. Quilliam, The insert region of RhoA is essential for Rho kinase activation and cellular transformation. *Mol. Cell. Biol.* **21**, 5287–5298 (2001).
34. J. L. Freeman, J. D. Lambeth, NADPH oxidase activity is independent of p47phox in vitro. *J. Biol. Chem.* **271**, 22578–22582 (1996).
35. R. Rose *et al*., Structural and mechanistic insights into the interaction between Rho and mammalian Dia. *Nature* **435**, 513–518 (2005).
36. S. Kühn *et al*., The structure of FMNL2-Cdc42 yields insights into the mechanism of lamellipodia and filopodia formation. *Nat. Commun.* **6**, 7088 (2015).
37. M. Lammers, S. Meyer, D. Kühlmann, A. Wittinghofer, Specificity of interactions between mDia isoforms and Rho proteins. *J. Biol. Chem.* **283**, 35236–35246 (2008).
38. H. Xu *et al*., Innate immune sensing of bacterial modifications of Rho GTPases by the Pyrin inflammasome. *Nature* **513**, 237–241 (2014).
39. D. R. Ambruso *et al*., Human neutrophil immunodeficiency syndrome is associated with an inhibitory Rac2 mutation. *Proc. Natl. Acad. Sci. U.S.A.* **97**, 4654–4659 (2000).
40. A. G. Kurkchubasche, J. A. Panepinto, T. F. Tracy, Jr, G. W. Thurman, D. R. Ambruso, Clinical features of a human Rac2 mutation: A complex neutrophil dysfunction disease. *J. Pediatr.* **139**, 141–147 (2001).
41. E. A. Lynch, J. Stall, G. Schmidt, P. Chavrier, C. D'Souza-Schorey, Proteasome-mediated degradation of Rac1-GTP during epithelial cell scattering. *Mol. Biol. Cell* **17**, 2236–2242 (2006).
42. A. J. McCoy *et al*., Phaser crystallographic software. *J. Appl. Cryst.* **40**, 658–674 (2007).
43. P. Emsley, B. Lohkamp, W. G. Scott, K. Cowtan, Features and development of Coot. *Acta Crystallogr. D Biol. Crystallogr.* **66**, 486–501 (2010).
44. G. Bricogne *et al*., BUSTER version X.Y.Z. Cambridge (Global Phasing Ltd., United Kingdom, 2016).
45. J. Siebourg-Polster *et al*., NEMix: Single-cell nested effects models for probabilistic pathway stimulation. *PLOS Comput. Biol.* **11**, e1004078 (2015).
46. M. Kearse *et al*., Geneious Basic: An integrated and extendable desktop software platform for the organization and analysis of sequence data. *Bioinformatics* **28**, 1647–1649 (2012).